Analysis of the AO-FDPC Optical Heterodyne Technique for Microwave Time Delay and Phased Array Beamsteering Applications

William D. Jemison, *Senior Member, IEEE*

***Abstract*—This paper presents a theoretical analysis of the application of the acousto-optic frequency-dependent phase compensated (AO-FDPC) optical heterodyne technique for microwave time delay applications and phased array beamsteering. A primary goal of the paper is to resolve open questions that have been associated with this interesting and highly referenced technique. The work presented here quantifies, for the first time, the fundamental time delay performance bounds of this technique in terms of the parameters associated with the AO-FDPC acousto-optic (AO) cell and the signal bandwidth. The theory presented in this paper is used to interpret previously reported experimental results that have been subject to debate. Much of the theoretical approach is general and may, therefore, be modified to address the design of new FDPC approaches. Finally, the wide-band beamsteering performance that can be achieved with this technique is quantified in terms of the AO cell parameters and phased array specifications.**

***Index Terms*—Optical heterodyne, phased array antennas, true-time delay.**

I. Introduction

THERE HAS been much interest in the use of microwave photonics for signal distribution in phased array antennas. Applications of microwave photonics have been proposed for various array signal-processing applications including signal distribution, phase shifting, and time delay generation. The utilization of photonics for time delay generation for wide-band phased array beamsteering is particularly appealing since RF delay lines are generally large, bulky, and heavy. An excellent review of optically generated true time delay (TTD) techniques is presented by Frigyes and Seeds [1]. While Frigyes and Seeds review the acousto-optic frequency-dependent phase compensated (AO-FDPC) time-delay technique in their work, they also point out that "questions remain still to be answered" regarding this technique. A primary purpose of this paper is to resolve these open questions. Therefore, it is appropriate to start with a brief discussion of how time delays may be generated.

Since the distance a wave travels d is equal to the product of the velocity of propagation ν and the transit time t, the total time differential may be easily derived as

$$\Delta t(d,\nu) = \frac{1}{\nu}\Delta d - \frac{d}{\nu^2}\Delta\nu. \tag{1}$$

Manuscript received September 6, 2000.

The author is with the Department of Electrical and Computer Engineering, Lafayette College, Easton, PA 18042 USA (e-mail: w.d.Jemison@ieee.org).

Publisher Item Identifier 10.1109/TMTT.2002.800446.

This equation clearly shows that time delay may be physically obtained in one of two primary ways. First, the distance the wave travels may be increased from d to $d+\Delta d$ without changing the velocity of propagation ($\Delta\nu = 0$). This approach may be used to realize either continuous or discrete delays. Continuous time delays have been demonstrated using fiber stretching techniques [2] and chirped fiber gratings [3], [4]. Discrete delays may be achieved via a switched line approach. Switched optical time-delay lines have been proposed using various switching methods including optical cross-bar switches [5], [6], thick retroreflective gratings [7], waveguide-coupled MSM detectors [8], deformable mirror devices [9], semiconductor switches [10], coherent optical detection [11], and acousto-optic (AO) deflection [12]. Switched line techniques have also been implemented in optical heterodyne systems via the use of spatial light modulators (SLMs) to realize a fixed number of discrete time delays [13], [14].

The second way to introduce a differential time delay is to change the velocity of propagation from ν to $\nu + \Delta\nu$ (where $\Delta\nu$ is negative) while keeping the propagation distance constant ($\Delta d = 0$). This approach has found application in optically controlled millimeter-wave plasma phase shifters [15] and microwave time-delay units employing highly dispersive optical fibers in conjunction with frequency tunable lasers [16]–[18].

Theoretically, a time delay may also be implemented via the time shifting property of the Fourier transform whose general form is given below:

$$x(t-t_o) \overset{FT}{\Leftrightarrow} e^{-j\omega t_o}X(j\omega). \tag{2}$$

This equation shows that a signal $x(t)$ may be delayed by t_o seconds by applying a frequency-dependent phase compensation (FDPC) $e^{-j\omega t_o}$ to the frequency spectrum $X(j\omega)$ of the signal. Several researchers have proposed the use of FDPC within an optical heterodyne system to realize a continuously variable time delay. For the purposes of this paper, this general approach will be called the FDPC heterodyne technique. A specific implementation of this approach that uses an AO cell to implement FDPC in the optical domain will called the AO-FDPC heterodyne technique. The FDPC heterodyne techniques are particularly appealing since programmable continuously variable time delays are possible and the parallelism of optical signal processing may potentially be exploited to simultaneously control the time delay of multiple phased array elements. Toughlian and Zmuda utilized the AO-FDPC

heterodyne technique [19]–[21] and were the first to experimentally demonstrate its time-delay generation. Maak *et al.* also have presented experimental time-delay results using the AO-FDPC heterodyne technique [22]. Stillwell *et al.* proposed a A0-FDPC time-delay system that used complementary discriminator circuits; however, experimental time-delay results were not presented [23], [24]. Frigyes *et al.* also provided analysis and simulation of two AO-FDPC approaches [25].

While most optical heterodyne systems are well understood [13], [14], [26]–[30], there are still open questions regarding the fundamental origin and limitations of the time-delay mechanism in an AO-FDPC heterodyne system. Another question that remains open is the issue as to whether or not the experimental results obtained in an AO-FDPC heterodyne system at a single frequency are due to a time-delay mechanism or a phase-shifting mechanism. Since time delay and phase shift are indistinguishable for a single-frequency signal, the interpretation of a multiple 2π phase shift as a multiple wavelength TTD [18], [19] has added to the questions surrounding the AO-AO-FDPC technique. Finally, the wide-band or time-delay phased array system beamsteering (i.e., squint free) performance that can be achieved via the application of the AO-FDPC technique has not been addressed. Time-delay beamsteering is typically required for phased array applications when the array is either electrically large and is scanned to wide angles or uses a wide instantaneous bandwidth.

In Section II, a full analysis of the AO-FDPC heterodyne technique is presented. While the analysis can be adapted to a general FDPC heterodyne system (which may not use an AO cell), it specifically addresses the AO-FDPC work of Toughlian and Zmuda [19]–[21]. It is useful to refer to their system since it is a mature and highly referenced realization of this time-delay technique and experimental results have been demonstrated. Monsay *et al.* have also previously addressed this work by recognizing the need to identify the cause of small oscillations that are superimposed on the output phase and addressing ways to increase the operating frequency [31]. The work presented in this paper fully addresses, for the first time, the origin and associated limitations of the AO-FDPC physical time-delay mechanism. The analysis presented specifically distinguishes between time delay and phase shift for an arbitrarily modulated signal and shows that both may result from the AO-FDPC heterodyne process. Also in Section II, an analysis is presented that quantifies the programmable time delay that can be achieved using this technique based on system hardware parameters. The pulse delay experiments reported by Toughlian and Zmuda are in excellent agreement with this theory, however, it is hypothesized that the multiple 2π phase shift obtained from their continuous wave experiments is due to a phase shift that can be predicted from the AO-FDPC system analysis rather than a TTD.

In Section III, the application of the AO-FDPC technique to wide-band (i.e., time delay) phased array beamsteering is analyzed. The results of this beamsteering analysis define the maximum number of phased array elements that can be supported by an AO-FDPC heterodyne system subject to key optical signal-processing component specifications and a maximum allowed level of phased array beam squint.

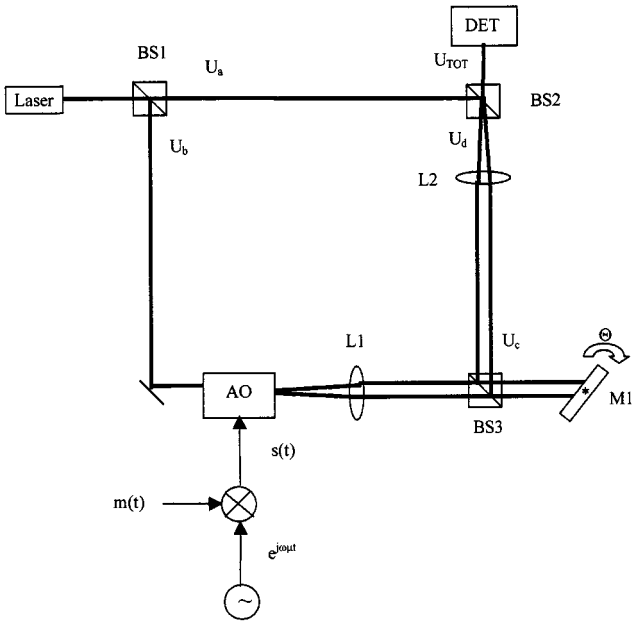

Fig. 1. *AO-FDPC* optical heterodyne system.

II. AO-FDPC Heterodyne System Analysis

In this section, the optical heterodyne system shown in Fig. 1 is theoretically analyzed. This system includes the following optical signal-processing elements in the lower arm of the heterodyne system.

- A single sideband (SSB) frequency modulator to introduce the modulated microwave carrier signal (an AO cell is commonly used for this purpose).
- A rotational mirror (M1) to introduce frequency dependant phase compensation (for the purposes of this analysis, the angular rotation may be assumed to be small such that the reflected beam can be considered to be essentially parallel with the incident beam).

The effects of these signal-processing elements on the properties of the microwave signal recovered at the output of the optical detector will be described. It should be noted that since a primary concern of this paper is the derivation of the phase-shift and time-delay properties of the AO-FDPC heterodyne system, it is assumed that all optical components are lossless. Furthermore, it is also assumed that the proper bias of the heterodyne system is maintained since the inclusion of the bias terms are not germane to the discussion of fundamental time-delay and phase-shifting properties and bias effects are well known [16]. The analysis proceeds using a complex wavefunction description (i.e., field representation) of the optical signals [32].

A. Signal Analysis of the AO-FDPC Performance

As shown in Fig. 1, the incident signal from the laser source of intensity U_o is separated into two beams using a beamsplitter, BS1, resulting in the following complex optical wavefunctions, $U_a(t)$ and $U_b(t)$, at the beamsplitter output

$$U_a(t) = \frac{U_o}{2} e^{j\omega_0 t} \tag{3a}$$

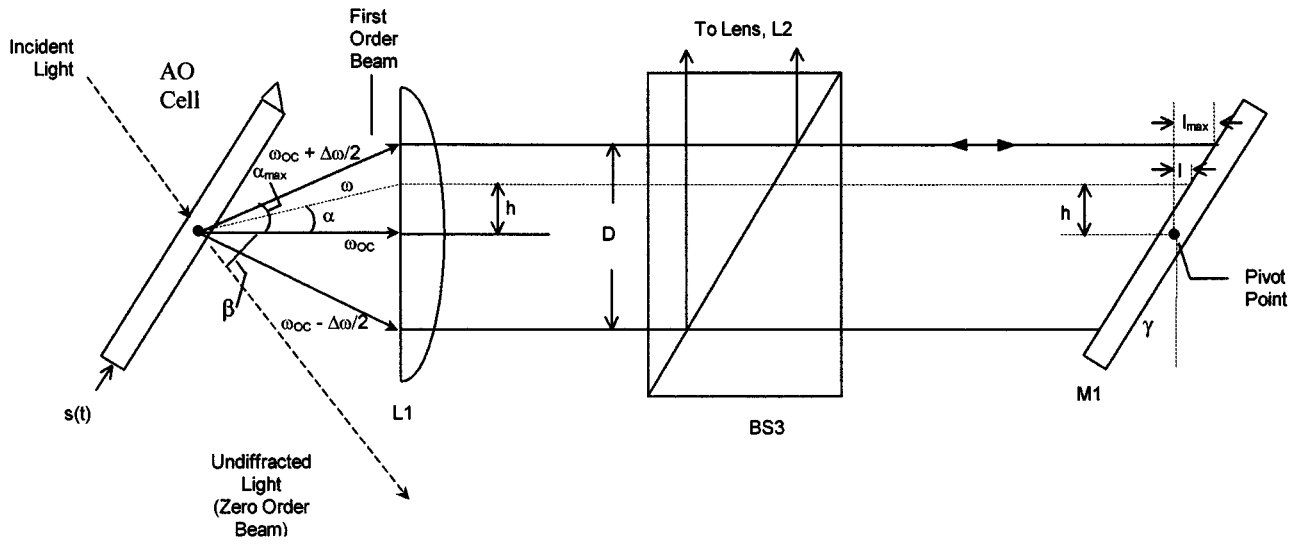

Fig. 2. Detail of rotational mirror operation.

$$U_b(t) = \frac{U_o}{2} e^{j\omega_0 t}. \tag{3b}$$

The optical signal $U_b(t)$ is then modulated by a microwave signal that is applied to the SSB modulator. In general, this microwave signal $s(t)$ is a microwave carrier at frequency $\omega_\mu + \delta\omega_\mu$ that is modulated by a baseband information signal $m(t)$

$$s(t) = m(t)e^{j(\omega_\mu + \delta\omega_\mu)t}. \tag{4}$$

The baseband information signal $m(t)$ may be complex as shown below such that both amplitude modulation (AM) and phase modulation (PM) may be considered

$$m(t) = |m(t)|e^{j\theta_m(t)}. \tag{5}$$

The baseband and microwave signals have Fourier transforms $M(j\omega)$ and $S(j\omega)$

$$m(t) \overset{FT}{\Leftrightarrow} M(j\omega) \tag{6}$$

$$s(t) \overset{FT}{\Leftrightarrow} S(j\omega). \tag{7}$$

The frequency shifting property of the Fourier transform allows $S(j\omega)$ to be expressed as

$$S(j\omega) = M(j(\omega - (\omega_\mu + \delta\omega_\mu))). \tag{8}$$

Typically, an AO cell is used as the SSB. At low RF power levels, the AO output light intensity is linearly proportional to the RF amplitude [32]. Thus, the output of the SSB modulator is

$$U_c(t) = s(t)\frac{U_o}{2} e^{j\omega_0 t}. \tag{9}$$

The AO cell will spatially separate the optical signal $U_c(t)$ into its composite frequency components, effectively performing a spatial Fourier transform. The lens L1, with focal length F, is used to stop the angular spread from the AO cell and to image the frequency components onto the mirror M1. Therefore, it is convenient to express $U_c(t)$ in the frequency domain as $U_c(j\omega)$. It is not necessary to explicitly include the spatial dependence since $U_c(j\omega)$ will ultimately be focused back down into a single optical beam by the lens L2. By applying the frequency shifting property of the Fourier transform in conjunction with (8) and (9), $U_c(j\omega)$ may be expressed as

$$U_c(j\omega) = \frac{U_o}{2} M(j(\omega - \omega_{oc} - \delta\omega_\mu)) \tag{10}$$

where ω_{oc} is the optical carrier associated with the nominal microwave frequency ω_μ.

Next, the effect of the rotational mirror, M1, must be accounted for. As shown in Fig. 2, the nominal beam diffraction angle β of the first-order beam is established by the microwave carrier frequency ω_μ. It should be noted that the optical carrier at ω_{oc} is aligned with the mirror pivot point. Also shown in Fig. 2 is the spread of the first order diffracted beam due to frequency deviations about ω_{oc}. These frequency deviations are due to the finite instantaneous bandwidth $\Delta\omega$ of the signal $s(t)$. The angle α associated with a particular instantaneous optical frequency component ω is directly proportional to the frequency deviation from ω_{oc} and is given by [20] where ν_{AO} is the velocity of propagation in the AO cell

$$\alpha = \frac{\lambda_o}{2\pi\nu_{\mathrm{AO}}}(\omega - \omega_{oc}). \tag{11}$$

The sign of α may be positive or negative depending on whether a positive or negative frequency deviation $\delta\omega_\mu$ from ω_{oc} is considered. The maximum magnitude of α is given by

$$\alpha_{\max} = \frac{\lambda_o}{2\pi\nu_{\mathrm{AO}}}\left(\frac{\Delta\omega}{2}\right). \tag{12}$$

The distance from the center of the beam associated with the optical frequency ω is given by

$$h = F\tan(\alpha) \tag{13}$$

where F is the focal length of the lens. The maximum magnitude of h is $D/2$ where D is the beam diameter.

The one-way optical path length change l associated with the optical frequency ω due to the mirror rotation is

$$l = h\tan(\gamma) \tag{14}$$

where γ is the angular rotation of the mirror. This value is referenced to the mirror pivot point that is located at the center of the mirror. The maximum magnitude of the l is given by

$$l_{\max} = \frac{D}{2}\tan(\gamma). \tag{15}$$

Substituting (11) into (13), (13) into (14), and applying small angle approximations for α and γ, results in the following approximation for l:

$$l \cong \frac{F\lambda_o\gamma}{2\pi\nu_{\mathrm{AO}}}(\omega - \omega_{oc}). \tag{16}$$

The round-trip (i.e., two-way) insertion phase associated with this path length change is a function of both the mirror rotation γ and the optical frequency ω and is computed as

$$\Phi_{\mathrm{opt}}(\gamma, \omega) = 2k_{oc}\frac{F\lambda_o\gamma}{2\pi\nu_{\mathrm{AO}}}(\omega - \omega_{oc}) \tag{17}$$

where k_{oc} is the wavenumber of the optical carrier ($k_{oc} = 2\pi/\lambda_{oc}$).

It should be stressed that the insertion phase given by (17) is on the order of that associated with several optical wavelengths (i.e., multiple π of phase shift in the optical domain). To highlight this fact, it is convenient to define a term $\delta z'$ as

$$\delta z' = \frac{F\lambda_o\gamma}{\pi\nu_{\mathrm{AO}}}. \tag{18}$$

This term has units of micrometers per megahertz (μm/MHz). It is not an absolute distance, but a "slope" that describes the change in the two-way path length introduced by the mirror rotation as a function of frequency. The product of $\delta z'$ and the angular frequency give the incremental path length introduced by the mirror for the optical frequency component ω under consideration.

In addition, it is also useful to normalize $l_{\max}$ given in (15) to the optical wavelength λ_o. This result gives the maximum two-way path length change associated with the band-edge frequency component $\pm\Delta f/2$ in terms of a number of optical wavelengths. This result $n_{\lambda o}$ is given below:

$$n_{\lambda o} = \frac{\gamma F\Delta f}{2\nu_{\mathrm{AO}}} \tag{19}$$

where $\Delta f = \Delta\omega/2\pi$ is the signal bandwidth. A practical value for $n_{\lambda o}$ is on the order of ten, indicating that the mirror is introducing ten optical wavelengths of delay and advance (i.e., on the order of 10^{-13} s) to the highest and lowest frequency components in the AO cell output spectrum, respectively.

Therefore, in general, the rotational mirror M1 imposes a phase function $\Phi_{\mathrm{opt}}(\gamma, \omega)$ that, for a given mirror rotation angle γ, is a linear function of the optical frequency ω as shown below:

$$\Phi_{\mathrm{opt}}(\gamma, \omega) = k_{oc}\delta z'\{\omega - (\omega_o + \omega_\mu)\}. \tag{20}$$

Since the phase function of (20) is dependent on the optical frequency, it provides "frequency-dependent phase compensation." The reference phase for any continuous wave microwave frequency is defined to be associated with a zero degree mirror tilt (i.e., $\gamma = 0$). It should be noted that when ω is equal to ω_{oc} (i.e., $\delta\omega_\mu = 0$), the phase function of (20) is zero regardless of the mirror tilt angle. This occurs because the optical frequency component under consideration (i.e., $\omega = \omega_{oc}$) is aligned with the mirror pivot point. However, continuous wave frequencies that are offset from ω_{oc} by $\delta\omega_\mu$ experience a phase shift relative to their reference phase that changes with the mirror rotation.

The signal at the output of the rotational mirror, $U_d(j\omega)$, may be expressed in terms of the optical insertion phase function $\Phi_{\mathrm{opt}}(\gamma, \omega)$

$$U_d(j\omega) = U_c(j\omega)e^{-j\Phi_{\mathrm{opt}}(\gamma,\omega)}. \tag{21}$$

Substituting (20) into (21) gives the following result:

$$U_d(j\omega) = U_c(j\omega)e^{-jk_{oc}\delta z'(\omega-\omega_{oc})}. \tag{22}$$

Next, the lens L2 focuses the light back into a single optical beam, making it more convenient to use a time-domain signal representation. The inverse Fourier transform of $U_d(j\omega)$ may be accomplished by letting $\tau = k_{oc}\delta z'$ and invoking the time shifting property of the Fourier transform. The following time-domain result for the optical wavefunction, $U_d(t)$ is obtained:

$$U_d(t) = U_c(t-\tau)e^{j\omega_{oc}\tau}. \tag{23}$$

Applying (4), (5), and (9) to (23) yields the following result for $U_d(t)$:

$$U_d(t) = \frac{U_o}{2}|m(t-\tau)|e^{j\omega_o t}e^{j\omega_\mu t}e^{j\theta_m(t-\tau)}e^{j\delta\omega_\mu(t-\tau)}. \tag{24}$$

As expected, $U_d(t)$ is a function of the rotation of the mirror, the microwave carrier frequency, and the AM and PM modulation of the baseband signal.

Finally, the signals from each arm of the interferometer are combined in beamsplitter BS2 to complete the heterodyne process such that the total optical field U_T illuminating the optical detector is

$$U_T(t) = U_a(t) + U_d(t). \tag{25}$$

The output photocurrent of the optical detector $I(t)$ is proportional to the magnitude squared of the total optical field [32]

$$I(t) \propto U_T(t)U_T^*(t). \tag{26}$$

Performing this calculation and retaining only the high frequency component gives the microwave frequency photodetector output current

$$I(t) \propto \frac{U_o^2}{2}|m(t-\tau)|\cos((\omega_\mu+\delta\omega_\mu)t+\theta_m(t-\tau)-\varphi). \tag{27}$$

It should be noted that the AO-FDPC heterodyne process results in both a time delay τ and a phase shift φ of the complex envelope of the microwave signal. The time delay τ, introduced by the AO-FDPC heterodyne system, is given by

$$\tau = k_{oc}\delta z' \tag{28}$$

and the microwave phase shift φ is given by

$$\varphi = \delta\omega_\mu \tau. \tag{29}$$

It should be further noted that while the time delay introduced by the mirror rotation is on the order of the period of the optical carrier $2\pi/\omega_o$, the time delay τ is on the order of the period of the microwave carrier $2\pi/\omega_\mu$. Moreover, the time delay is programmable since it is a function of the rotation of the mirror M1. The phase is both a function of the mirror rotation through the time-delay term τ and the microwave carrier frequency shift $\delta\omega_\mu$.

Taken by itself, the previous signal analysis indicates that a large time delay on the order of the period of the microwave frequency ($\sim 10^{-9}$ s) results from the application of a small time delay on the order of the period of the optical frequency ($\sim 10^{-14}$ s). Intuitively, this cannot be the case. The following sections discuss several practical criteria that must be considered in conjunction with the previous analysis in order to properly understand the physical origin and associated limitations of AO-FDPC generated time delays that are larger than the optical period.

B. Physical Delay Mechanism and Bandwidth Constraints

As pointed out by Zmuda and Toughlian [20], the time delay associated with the AO-FDPC heterodyne system is a function of both the rotation of the mirror M1 and the energy storage (i.e., time delay) mechanism of the AO cell. The phase function introduced by the rotation of the mirror M1 effectively implements the frequency-dependent phase compensation required by the time shifting property of the Fourier Transform given in (2). However, it must be stressed that implicit in the integral associated with (2) are two related and critical conditions. First, all signal spectral components $X(j\omega)$ must be available for the full temporal duration of the signal $x(t)$, including the delay time. Second, the frequency-dependent phase compensation $e^{j\omega t_o}$ must be applied to the full spectrum $X(j\omega)$ for the entire signal duration (including the delay time). Therefore, a real-time hardware implementation of the Fourier transform time-delay property requires the following:

- an energy storage mechanism that can "store" the signal for the required time-delay duration;
- a spectral processor that can compute and provide the complete signal spectrum for the required time-delay duration;
- a frequency-dependent phase compensator that can apply the necessary frequency domain signal processing to the complete signal spectrum for the required time-delay duration.

Thus time delay does not result from frequency-dependent phase compensation alone. The signal analysis presented in Section II-A must be coupled with the simultaneous requirements of energy storage, complete spectral computation, and frequency-dependent phase compensation outlined above in order to physically realize a TTD.

When these concepts are applied to the AO-FDPC heterodyne system, it is readily recognized that time delay is possible only when the signal to be delayed is fully contained in the AO cell active region d_{AO}. This is the only condition where the full signal spectrum will be available at the AO cell output. Conversely, time delay cannot be obtained when the signal is not fully contained in the AO cell active region. This implies the following two cases:

Case a) $T < t_{\mathrm{AO}}$

Case b) $T > t_{\mathrm{AO}}$.

T is the signal pulse duration and t_{AO} is the transit time through the AO cell active region given by

$$t_{\mathrm{AO}} = \frac{d_{\mathrm{AO}}}{\nu_{\mathrm{AO}}}. \tag{30}$$

In this equation, d_{AO} is the length of the active region of the AO cell (i.e., the portion of the AO cell illuminated by the laser) and ν_{AO} is the velocity of propagation in the AO cell (typically five orders of magnitude slower than the speed of light).

Case a) is illustrated in Fig. 3(a) where the pulse duration T is less than transit time through the active region of the AO cell. In this case, the signal is fully contained in the active region of the AO cell. Hence, the required frequency spectrum is available at the AO cell output for frequency-dependent phase processing by the mirror M1.

Case b) is illustrated in Fig. 3(b). Here, the pulse duration is much longer than the transit time through the active region. At the instant in time shown, the pulse excitation appears as a CW signal to the AO cell and the instantaneous frequency spectrum is, therefore, identical to that of a single-frequency waveform (i.e., a single deflected beam), not a pulsed waveform. In this

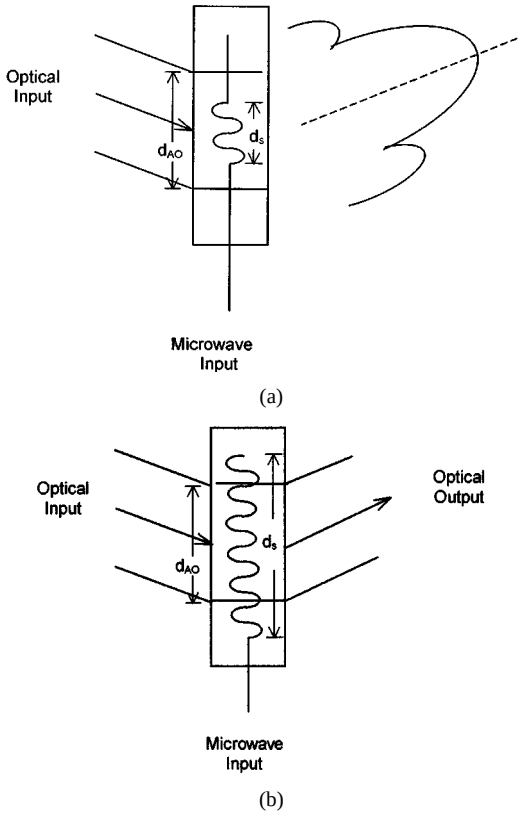

Fig. 3. (a) Signal duration less than AO transit time. (b) Signal duration greater than AO transit time.

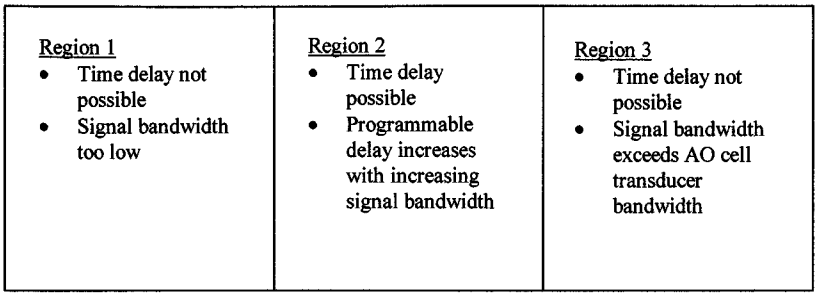

Fig. 4. Three regions of *AO-FDPC* heterodyne system operation.

case, the conditions implicit in the Fourier time-delay theory of (3a) are not satisfied and time delay cannot be produced.

It is most convenient to define the time-delay constraints in terms of the signal bandwidth. Since the bandwidth of the signal $\Delta f = \Delta\omega/2\pi$ is inversely proportional to the signal pulse duration T, the following condition must be satisfied in order to achieve time delay:

$$\frac{v_{\mathrm{AO}}}{d_{\mathrm{AO}}} \leq \Delta f \leq BW_{\mathrm{AO}}. \tag{31}$$

The first inequality defines the conditions outlined in Cases a) and b) discussed above. The second inequality ensures that the signal bandwidth be less than the AO cell transducer bandwidth, BW_{AO}; a requirement to maintain signal fidelity.

C. Programmable Time-Delay Limitations

Given that the signal bandwidth limitations have been defined, it is now important to quantify the amount of programmable time delay that can be realized by the AO-FDPC optical heterodyne system. First, since the AO cell is the energy storage medium for the time delay, the maximum delay that can be achieved will be a function of the signal transit time through the active region of the AO cell as noted by Toughlian and Zmuda [20]. However, it also must be recognized that if the duration of the pulsed signal is exactly matched to the AO cell transit time, the full frequency spectrum of the pulsed signal is available only at a single instant in time and programmable time delay is not possible as per the discussion in Section II-B.

Therefore, in order to achieve a programmable time delay, the duration of the pulsed signal must be shorter than the transit time through the AO cell. Under this condition, the spectral components required by the AO-FDPC time-delay processor are available for the finite amount of time necessary to implement the time delay. Recalling that the duration of the pulse waveform considered is inversely proportional to the pulse waveform bandwidth Δf (for the pulse waveform under consideration), the maximum amount of programmable delay that is possible, $\tau_{\max}$, is, therefore, the difference between the transit time and the duration of the pulse as shown below:

$$\tau_{\max} = t_{\mathrm{AO}} - T. \tag{32}$$

While the maximum angle of rotation of the mirror M1 will also affect the maximum delay, it is not expected to be a limiting element since fairly large rotations relative to the optical wavelength are possible.

Equations (31) and (32) define three distinct AO-FDPC heterodyne system regions of operation as shown in Fig. 4. In region 1 no TTD is possible since the signal bandwidth is not high enough support the pulse being fully contained in the AO cell active region. In region 2, time delay is possible and the maximum programmable time delay increases as the pulse width becomes narrower and the required signal spectral components are available for longer a duration. In region 3 the signal bandwidth has exceeded the transducer bandwidth of the AO cell and distortion-free time delay is no longer possible. Finally, it reassuring to note that velocity reduction experienced by the signal in the AO cell provides the energy storage in the system, thus maintaining consistency with the physical time-delay mechanisms predicted by (1).

D. Interpretation of Previous Experimental Time-Delay Results

The previous analyses are consistent with the two experiments conducted by Zmuda and Toughlian [19]–[21]. In the first experiment an impulse was used to excite an AO cell which had a 70-MHz center frequency (f_o), a 25-MHz bandwidth (Δf), a 0.6-mm active region (d_{AO}), and an acoustic velocity of 4000 m/s (ν_{AO}). The AO cell can, therefore, support a maximum signal bandwidth of 36% ($\Delta f/fo \times 100$). Since an impulse was used to excite the full 25-MHz bandwidth of the AO cell, a maximum delay $\tau_{\max}$, of 110 ns is predicted from (31) and (32) which compares closely with the 100-ns delay reported. It should be noted that there are several definitions of bandwidth [33]. A definition other than the unity time-bandwidth product one used here would result in even closer agreement. The maximum programmable time delay that can be achieved using this AO cell as given by (31) and (32) is plotted in Fig. 5 as a function of the percent bandwidth of the signal. This plot has the three distinct regions previously mentioned.

In a second experiment, a multiple 2π phase shift resulting from the application of a single-frequency applied to the AO cell was interpreted as a large time delay [19]–[21]. As previously mentioned, time delay and phase shift are indistinguishable for a single-frequency signal. Since the bandwidth of a single-frequency tone is effectively zero, (31) is not satisfied. Therefore, the observed phase shift must not be a result of TTD, but of a different mechanism. The previous system analysis clearly indicates that the AO-FDPC heterodyne system produces both time delay and phase shift. Equation (27) shows that the mirror rotation introduces a continuously variable phase shift through the term φ [see (29)] if the microwave carrier frequency is offset

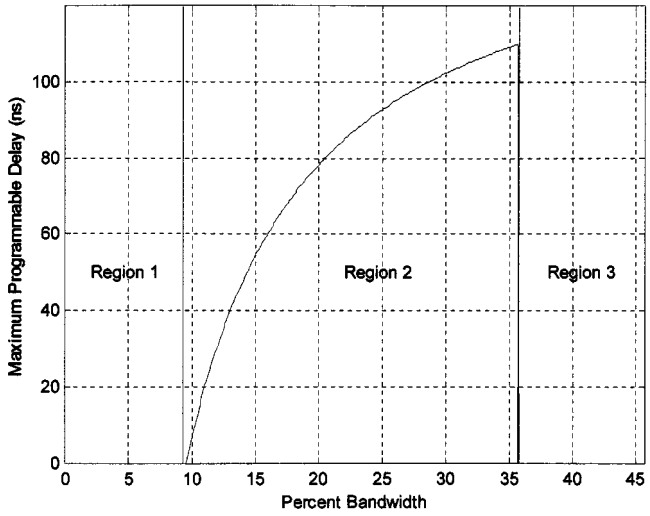

Fig. 5. Maximum programmable time delay as a function of percent signal bandwidth.

from ω_μ by an amount $\delta\omega_\mu$ (i.e., the beam is not exactly aligned with the mirror pivot point) Under this single-frequency condition, the system effectively operates as the well-known phase-shifting heterodyne system [26], resulting in a phase shift of the detected microwave carrier. Since the analysis presented here was not available at the time the experiments were performed, it is probable that the output beam was not exactly aligned with the mirror pivot point. Therefore, it is hypothesized that the observed single-frequency experimental result is not the result of TTD, but rather a result of a phase shift that can be predicted from the system analysis presented here.

Finally, it should be noted that the proposed frequency-dependent phase compensated heterodyne system which uses an optical grating [19] to perform the spatial Fourier transform cannot provide time delay unless the system includes an energy storage mechanism in a similar fashion as the AO cell. The rotation of the mirror by itself without an energy storage mechanism cannot produce a time delay. This restriction applies to other FDPC heterodyne time-delay configurations as well [23], [24]. In the next section, the application of the AO-FDPC heterodyne system will be analyzed with respect to phased array beamsteering.

III. Application of the AO-FDPC System to Phased Arrays

In the previous section, an analysis was presented that quantifies, via (31) and (32), the maximum programmable time delay that can be realized by the AO-FDPC heterodyne technique in terms of both the AO cell specifications and signal modulation bandwidth. Since the ultimate application of this heterodyne technique is phased array beamsteering, it is equally important to quantify the beamsteering performance that can be supported by this system approach. In this section, beamsteering performance specifications will be briefly discussed followed by an analysis that allows the AO-FDPC beamsteering performance to be quantified based on beamsteering specifications and the AO-FDPC hardware.

A. Wide-Band Beamsteering Performance Specifications

Practically, phased array beamsteering may be implemented using one of the three options listed below:

1) phase shifters at each element (phase-only steering);
2) sub-arrayed elements (phase and time-delay steering);
3) true-time delay (TTD) units at each element (time-delay-only beamsteering).

The latter two options can support wide-band beamsteering which is distinguished from narrow-band or phase-only beamsteering in that the antenna beam remains pointed in the same direction for a specified range of microwave frequencies. In other words, the beam does not squint with a change in frequency. Alternatively, it may be said that the antenna beam does not experience spatial dispersion when transmitting or receiving signals that have a wide instantaneous bandwidth.

It should be noted that beamsteering bandwidth may be limited by either aperture effects or feed effects as discussed by Cheston and Frank [34]. Only the aperture effect is considered in this analysis since it is fundamentally tied to the AO-FDPC heterodyne system architecture. In order to investigate the aperture bandwidth effect of the AO-FDPC heterodyne system, a simplified linear array geometry of consisting of contiguous, uniformly illuminated subarrays will be considered. The basic analysis technique is applicable, however, to a more complex array geometry such as those reviewed by Agrawal and Holzman [35].

The linear array shown in Fig. 6(a) consists of M subarrays, each having N elements spaced a distance s apart. The length of each subarray is $L_{\rm sub}$. Therefore, the total number of radiating elements is $M \times N$. Phase shifters are placed behind each element of the subarray and a TTD unit is placed behind each subarray. Special cases of this architecture include phase-only beamsteering in which there is only one subarray (i.e., N elements and no TTD steering) and time-delay-only beamsteering in which there is only one element per subarray (i.e., M elements with TTD units behind each element). These special cases are shown in Fig. 6(b) and (c), respectively.

When a wide-band signal is applied to the array the subarray pattern will experience beam squint, resulting in an effective loss of array gain over the signal bandwidth [34]. In addition, the array pattern will exhibit grating lobes due to discretized phase and time-delay progression across the array due to the subarrayed geometry. Both the loss in gain and grating lobe levels are dependent on the specific beamsteering angle and both typically get worse with increasing steering angle. Therefore, beamsteering performance may be specified by the

- maximum allowable main beam gain loss over the instantaneous signal bandwidth;
- maximum allowable grating lobe level;
- maximum scan angle at which either of the previous two conditions are specified.

For this analysis, it is assumed that gain degradation is the more critical of the first two specifications listed above. Therefore, the beamsteering performance of the AO-FDPC heterodyne system will be quantified based on the maximum allowable main beam gain loss at a specified maximum scan angle. Specifically, the following approach is used to quantify the AO-FDPC beamsteering performance:

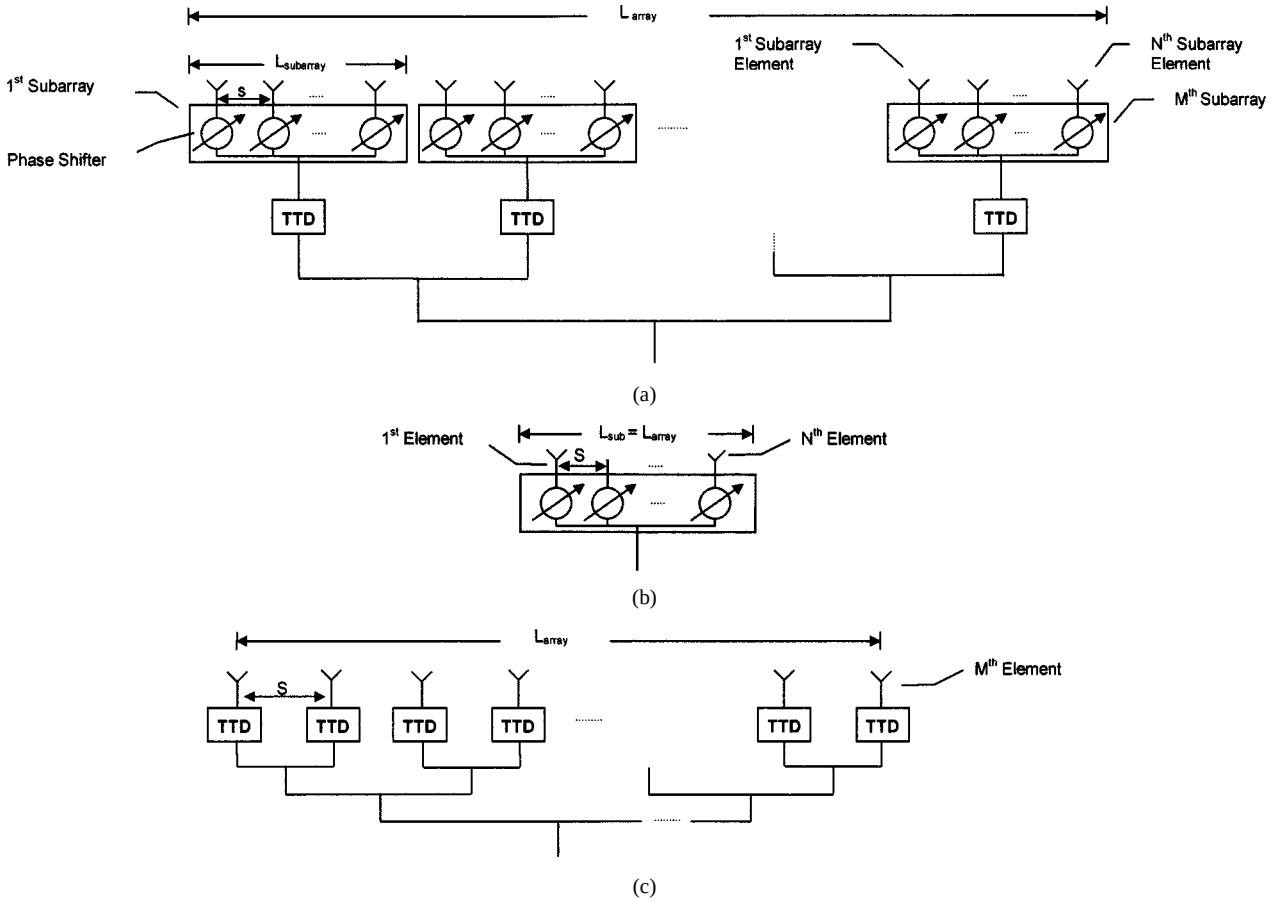

Fig. 6. (a) Generalized subarrayed architecture used for analysis. (b) Special Case 1: Phase-only steering ($M = 1$). (c) Special Case 2: Time-delay-only steering ($N = 1$).

1) specify the maximum allowable mainbeam gain loss for a given signal bandwidth and maximum beamsteering angle;
2) determine the subarray beamwidth and number of subarray elements that will support the previous gain loss specification;
3) determine the number of subarrays (i.e., array size) that can be used based on the maximum time delay that can be supported by the *AO-FDPC* hardware.

Once these steps have been completed, the array beamwidth and grating lobe levels are easily calculated, if desired. It should be noted that an alternate approach is to define the array size and bandwidth specification and then to define the time delay needed from *AO-FDPC* hardware. The first approach was taken since the maximum number of array elements is a useful measure of the practicality of a particular design as will be demonstrated in the following section.

B. Quantification of AO-FDPC Heterodyne Wide-Band Beamsteering

The first step in quantifying the wide-band beamsteering performance is to specify the maximum allowable main beam gain loss over the instantaneous frequency band at a maximum beamsteering angle. The loss in mainbeam gain at the edge of the instantaneous frequency band is given by [34]

$$\Delta G\,(\mathrm{dB}) = 20\log\left[\frac{\sin\left(\frac{\pi}{4}K\sin\theta_o\right)}{\frac{\pi}{4}K\sin\theta_o}\right] \tag{33}$$

where θ_o is the desired beamsteering angle and K is a bandwidth factor that is the ratio of the percent bandwidth $BW(\%)$ to the broadside subarray beamwidth θ_{sub} as shown below:

$$K = \frac{\mathrm{BW}(\%)}{\theta_{\mathrm{sub}}}. \tag{34}$$

The percent bandwidth $BW(\%)$ is given by

$$\mathrm{BW}(\%) = 100\,\frac{\Delta f}{f_o} \tag{35}$$

where Δf and f_o are the instantaneous bandwidth and the carrier frequency of the signal, respectively. Given this loss specification and the system percent bandwidth, (33) may be numerically solved to determine the bandwidth factor K that meets these requirements. Next, the subarray 3-dB beamwidth (in degrees) θ_{sub} may be determined from (34) for a specified percent bandwidth. The subarray length, L_{sub}, may then be determined for the uniformly illuminated subarrays considered here

$$L_{\mathrm{sub}} = 50.1\frac{\lambda_c}{\theta_{\mathrm{sub}}} \tag{36}$$

where λ_c is the wavelength at the carrier frequency.

The number of elements required in the subarray may now be computed by dividing the length of the subarray by the interelement distance s

$$N = \text{floor}\left(\frac{L_{\text{sub}}}{s}\right). \tag{37}$$

The floor( ) operator indicates rounding down to the nearest integer value of N. At this point, it should be noted that the maximum beamsteering angle that was specified for the array is directly related to the maximum array fill time. The array fill time at the maximum scan angle, therefore, determines the maximum time delay that must be delivered by the TTD unit. The maximum array fill time $T_{\max}$ is dependent on the electrical length of the array and may computed as

$$T_{\max} = \frac{N(M-1)L_{\text{sub}}}{c}\sin\theta_{o\max} \tag{38}$$

where c is the speed of light, L_{sub} is the subarray length, and $\Theta_{o\max}$ is the specified maximum beamsteering angle. Therefore, the number of subarrays that can be used while maintaining the beamsteering specifications may be computed by solving by (38) for M and substituting for N using (28). The result is shown below:

$$M = \text{floor}\left(\frac{cT_{\max}}{sN\sin\theta_{o\max}} + 1\right). \tag{39}$$

The total number of array elements N_e that can be used while maintaining the wide-band steering specifications is, therefore, the product of N and M

$$N_e = NM. \tag{40}$$

At this point, (32) and (36) may be substituted into (39) to determine the maximum number of array elements as a function of the *AO-FDPC* time-delay limitations, array parameters, and beamsteering bandwidth specification. The maximum number of elements for the subarrayed beamsteering architecture is given below:

$$N_e = \text{floor}\left(\frac{50.1\lambda_c K}{s}\right)\text{floor}\left(\frac{c\left(\frac{d_{\text{AO}}}{\nu_{\text{AO}}} - \frac{1}{\Delta f}\right)}{\text{sfloor}\left(\frac{50.1\lambda_c K}{s}\right)\sin\theta_{o\max}} + 1\right)$$

for sub-arrays. (41)

For the special cases of TTD-only beamsteering and phase-only steering, the total number of array elements is given by M and N, respectively. Note that these numbers will be different from the values of N and M computed for the subarrayed architecture since they correspond to fundamentally different types of array configurations. These can be written in terms of the same variables used above

$$M = \text{floor}\left(\frac{c\left(\frac{d_{\text{AO}}}{\nu_{\text{AO}}} - \frac{1}{\Delta f}\right)}{s\sin\theta_{o\max}} + 1\right)$$

for time-delay-only steering (42)

$$N = \text{floor}\left(\frac{50.1\lambda_c K}{s}\right)$$

for phase-only steering. (43)

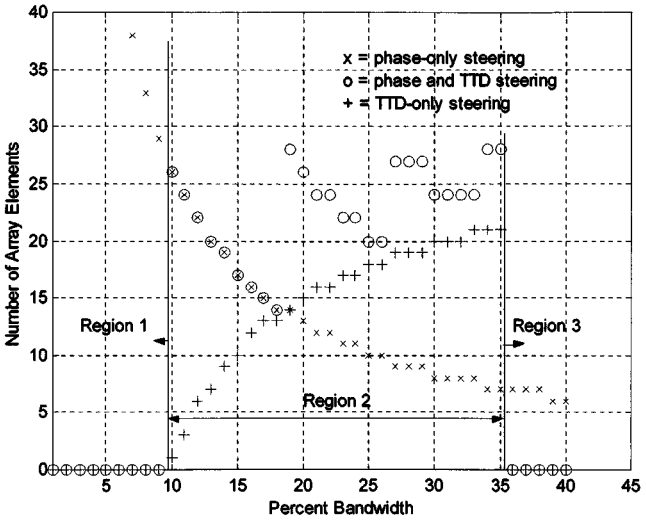

Fig. 7. Maximum number of array elements for Case Study 1.

It should be noted that the total number of array elements for the subarrayed architecture is a function of both the AO cell (i.e., TTD unit) properties, the bandwidth parameter K associated with the gain loss specification, as well as a number of the array parameters (e.g., element spacing). The total number of array elements for the time-delay steering only method is independent of the bandwidth factor K since this architecture does not experience gain loss due to beam squint. Likewise, the total number of array elements associated with the phase only beamsteering approach is independent of the AO cell parameters since it does not employ time-delay units. If desired, the array beamwidth and the grating lobes generated by the resulting array geometry may now be computed by the method presented by Mailloux [36].

Equations (41)–(43), may be plotted as a function of the percentage bandwidth of the transmitted (or received) signal for given beamsteering and *AO-FDPC* hardware specifications to determine if the number of array elements supported by the *AO-FDPC* phased array architecture is feasible and/or useful. In the next section, two cases will be presented to explore the utility of the *AO-FDPC* heterodyne method for practical arrays.

C. Case Study of Specific AO-FDPC Architectures

In the case studies, the following beamsteering specifications were used. First, the specification for the main beam gain loss is 0.8 dB. This value corresponds to the radar pulsewidth being equal to the aperture fill time as discussed in [34]. Second, the beamsteering angle at which this loss is specified, $\theta_{o\max}$, was chosen to be 45°. While these specifications are somewhat arbitrary, they are representative of specifications for practical arrays.

1) Case Study Number 1: In this case, the AO cell specifications given by Toughlian and Zmuda were used [19]. The AO cell had a 70-MHz center frequency, a 25-MHz bandwidth, a 0.6-mm active region, and an acoustic velocity of 4000 m/s. Equations (32)–(34) are plotted in Fig. 7 to show the number of array elements that can be supported by the *AO-FDPC* system as a function of the percent bandwidth of the transmitted signal.

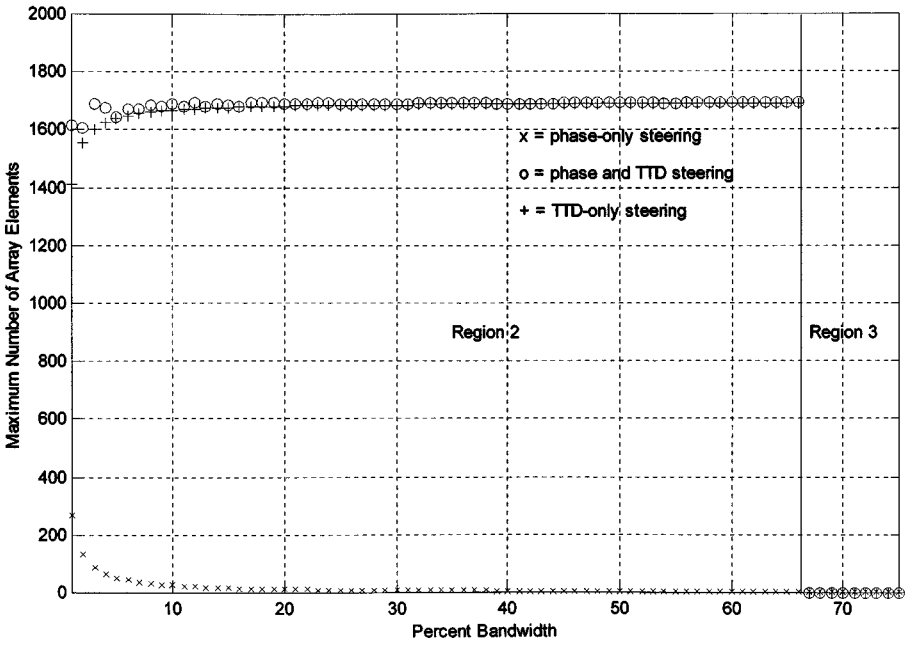

Fig. 8. Maximum number of array elements for Case Study 2.

TABLE I
CASE STUDY SYSTEM PARAMETERS

Parameter	System 1	System 2
Center Frequency, f_o (MHz)	70	3000
AO Cell Bandwidth, Δf (MHz)	25	2000
Percent Bandwidth (%)	35.7	66.7
Acoustic Velocity, v_{AO} (m/s)	4000	3440
Active Length, d_{AO} (mm)	0.6	0.688
Transit Time, t_{AO} (ns)	150	200
Maximum Time Delay, τ_{max} (ns)	110	199.5
Maximum Delay (wavelengths) = $f_o \tau_{max}$	10.5λ	600λ
Time Bandwidth Product = $t_{AO} \Delta f$	3.75	400

2) Case Study Number 2: In this case, a wide-band AO cell described by Riza was used [37]. The AO cell had a 3-GHz center frequency, a 2-GHz bandwidth, a 0.688-mm active region, and an acoustic velocity of 3440 m/s. Equations (41)–(43) are plotted in Fig. 8.

The system parameters associated with both case studies are summarized in Table I.

D. Discussion of Results

Figs. 7 and 8 show several interesting results. First, in both Figs. 7 and 8 the number of elements that can be supported for phase-only beamsteering (i.e., the $\times$s) drops dramatically as the percent bandwidth of the signal increases, as expected. However, the number of elements that can be supported for time-delay-only beamsteering (i.e., the os) is not independent of the percent bandwidth as would typically be expected for arrays using traditional time-delay elements such as variable-length transmission lines. This is due to the unique time-delay properties of *AO-FDPC* heterodyne system. Equations (31) and (32) clearly indicate that there is a restriction in the amount of time delay that can be achieved using the *AO-FDPC* technique that is associated with the percent bandwidth of the signal and the AO cell properties. Likewise, the time delays that may be achieved for a subarrayed architecture are restricted.

Furthermore, as shown in Fig. 7, the maximum number of array elements supported by the heterodyne system of case study 1 is very small. The maximum supported time delay of 110 ns is simply not large enough relative to the length of the array since it can only provide a 10.5λ delay. (Recall, the array operates at 70 MHz and uses half-wavelength element spacing.) Therefore, while this system is adequate for demonstration purposes, it will not support practical array designs. In case study 2, the AO cell has a 67% bandwidth and a time bandwidth product of 600 that supports a maximum delay of 600λ. Therefore, many array elements can be supported by a *AO-FDPC* heterodyne system using this AO cell. It must be stressed that the number of array elements plotted in Figs. 7 and 8 are maximum numbers based on a consideration of only of the amount of time delay that can be achieved in the *AO-FDPC* heterodyne system. Practically, a reduction in the number of elements will occur due to spatial constraints in the heterodyne

system imposed by the mechanical design as discussed by Riza [37].

IV. Conclusions

This paper presents a theoretical analysis of the microwave phase-shifting and time-delay performance of the AO-FDPC optical heterodyne system. The paper quantifies the physical time-delay mechanism and time-delay performance limitations of this technique in terms of the AO cell parameters and the signal bandwidth. Specifically, three distinct regions of operation are identified. In the first region, time delay is not possible because the signal bandwidth is too small. In the second region, time delay can be supported, but the amount of programmable delay is signal bandwidth dependent. In the third region, time delay cannot be supported because the signal bandwidth exceeds the AO cell transducer bandwidth. This unique type of operation may be useful in other applications for the temporal discrimination of signals based on bandwidth. It is also shown that both time delay and phase shift may occur. The results are used to propose an interpretation of previously reported experimental results. Finally, the wide-band (i.e., squint free) phased array system beamsteering performance that can be achieved via the application of the AO-FDPC heterodyne technique is quantified. The results of this analysis give the maximum number of array elements that can be supported by an AO-FDPC heterodyne system. This number can vary widely depending on the AO cell specifications. This is demonstrated via the consideration of two different case studies. In summary, this work provides a greater understanding of both the fundamental theory of operation and the application of the highly referenced AO-FDPC heterodyne system to phased array antennas.

Acknowledgment

The author acknowledges several helpful discussions with Prof. P. R. Herczfeld, Drexel University, Philadelphia, PA.

References

[1] I. Frigyes and A. J. Seeds, "Optically generated true-time delay in phased array antennas," *IEEE Trans. Microwave Theory Tech.*, vol. 43, pp. 2378–2386, Sept. 1995.

[2] P. R. Herczfeld, A. S. Daryoush, M. Keili, S. Siegal, and R. Soref, "Wideband true time delay phase shifter devices," in *IEEE MTT-S Int. Microwave Symp. Dig.*, June 1987, pp. 603–606.

[3] J. L. Corral, J. Marti, S. Regidor, J. M. Fuster, R. Laming, and M. J. Cole, "Continuously variable true time-delay optical feeder for phased-array antenna employing chirped fiber gratings," *IEEE Trans. Microwave Theory Tech.*, vol. 45, pp. 1531–1536, Aug. 1997.

[4] Y. Chang, B. Tsap, H. R. Fetterman, D. A. Cohen, A. F. J. Levi, and I. R. Newberg, "Optically controlled serially fed phased-array transmitter," *IEEE Microwave Guided Wave Lett.*, vol. 7, pp. 69–71, Mar. 1997.

[5] E. Ackerman *et al.*, "Integrated 6-bit photonic true-time-delay unit for lightweight 3–6 GHz radar beamformer," in *IEEE AP-S Int. Symp. Dig.*, 1992, pp. 681–684.

[6] E. J. Murphy, T. F. Adda, W. J. Minford, R. W. Irvin, E. I. Ackerman, and S. B. Adams, "Guided-wave optical time delay network," *IEEE Photon. Technol. Lett.*, vol. 8, pp. 545–547, Apr. 1996.

[7] J. M. Florence, "Monolithic optical time shift network for phased arrays," in *IEEE AP-S Int. Microwave Symp. Dig.*, May 1990, pp. 782–785.

[8] W. Ng, D. Yap, A. Narayanan, and A. Walston, "High-precision detector-switched monolithic GaAs time-delay network for the optical control of phased arrays," *IEEE Photon. Technol. Lett.*, vol. 6, pp. 231–234, Feb. 1994.

[9] N. F. Hartman and L. E. Corey, "Integrated optic time delay network for phased array antennas," in *Proc. IEEE Int. Radar Conf.*, Mar. 1991, pp. 79–82.

[10] W. Ng, A. A. Walston, G. L. Tangonan, J. J. Lee, I. L. Newberg, and N. Bernstein, "The first demonstration of an optically steered microwave phased array antenna using true-time delay," *J. Lightwave Technol.*, vol. 9, pp. 1124–1131, Sept. 1991.

[11] L. Xu, R. Taylor, and S. R. Forrest, "The use of optically coherent detection techniques for true-time delay phased array systems," *J. Lightwave Technol.*, vol. 13, pp. 1663–1678, Aug. 1995.

[12] W. D. Jemison, T. Yost, and P. R. Herczfeld, "Acousto-optically controlled true time delays—Experimental results," *IEEE Microwave Guided Wave Lett.*, vol. 8, pp. 283–285, Aug. 1996.

[13] D. Dolfi *et al.*, "Optically controlled true time delays for phased array antennas," *SPIE Opt. Technol. Microwave Applicat. IV*, pp. 152–161, Mar. 1989.

[14] N. A. Riza, "Transmit/receive time-delay beam-forming optical architecture for phased array antennas," *Appl. Opt.*, vol. 30, no. 32, pp. 4594–4595, Nov. 1991.

[15] A. M. Vaucher, C. D. Striffler, and C. H. Lee, "Theory of optically controlled millimeter-wave phase shifters," *IEEE Trans. Microwave Theory Tech.*, vol. MTT-34, pp. 147–155, Jan. 1986.

[16] R. A. Soref, "Optical dispersion technique for time-delay beamsteering," *Appl. Opt.*, vol. 31, no. 35, pp. 7395–7397, Dec. 1992.

[17] M. Y. Frankel and R. D. Esman, "True time-delay fiber-optic control of an ultrawideband array transmitter/receiver with multibeam capability," *IEEE Trans. Microwave Theory Tech.*, vol. 43, pp. 2387–2394, Sept. 1995.

[18] H. Zmuda, E. N. Toughlian, P. Payson, and H. W. Klumpe, III, "A photonic implemenation of a wide-band nulling system for phased arrays," *IEEE Photon. Technol. Lett.*, vol. 10, pp. 725–727, May 1998.

[19] E. N. Toughlian and H. Zmuda, "A photonic variable RF delay line for phased array antennas," *J. Lightwave Technol.*, vol. 8, pp. 1824–1828, Dec. 1990.

[20] H. Zmuda and E. N. Toughlian, "Adaptive microwave signal processing: A photonic solution," *Microwave J.*, vol. 35, pp. 58–68, Feb. 1992.

[21] E. N. Toughlian and H. Zmuda, "Variable time delay for RF/microwave signal processing," *SPIE Opt. Technol. Microwave Applicat. V*, vol. 1476, pp. 107–121, 1991.

[22] P. Maak, J. Remenyi, L. Jakab, P. Tichter, I. Frigyes, and I. Habermayer, "True time delay line for short pulses based on optical path-length dispersion: Experimental proof of functioning," in *IEEE Int. Phased Array Sys. Technol. Conf.*, May 2000, pp. 449–452.

[23] D. Stillwell, M. Parent, and L. Goldberg, "Microwave time delay beamforming using optics," in *Proc. IEEE Nat. Radar Conf.* , 1991, pp. 50–53.

[24] ——, "Fiber optic feed," Naval Res. Lab., NRL Memo. Rep. 6741, Nov. 6, 1990.

[25] I. Frigyes, O. Schwelb, and J. Berces, "Investigations and improvements in microwave opto-electronic variable delay lines," in *IEEE MTT-S Int. Microwave Symp. Dig.*, vol. 2, June 1996, pp. 887–890.

[26] R. A. Soref, "Voltage controlled optical/RF phase shifter," *J. Lightwave Technol.*, vol. LT-3, pp. 992–998, 1985.

[27] G. A. Koepf, "Optical processor for phased-array antenna beam formation," *Proc. SPIE—Opt. Technol. Microwave Applicat.*, vol. 447, pp. 75–81, 1984.

[28] M. Tamburrini, M. Parent, L. Goldberg, and D. Stillwell, "Optical feed for a phased array microwave antenna," *Electron. Lett.*, vol. 23, no. 13, pp. 680–681, June 1987.

[29] E. N. Toughlian, H. Zmuda, and P. Kornreich, "A deformable mirror-based optical beamforming system for phased array antennas," *IEEE Photon. Technol. Lett.*, vol. 2, pp. 444–446, June 1990.

[30] N. A. Riza and D. Psaltic, "Acousto-optic signal processors for transmission and recption of phased-array antenna signals," *Appl. Opt.*, vol. 30, no. 23, pp. 3294–3303, Aug. 1991.

[31] E. H. Monsay, K. C. Baldwin, and M. J. Caccuitto, "Photonic true time delay for high-frequency phased array systems," *IEEE Photon. Technol. Lett.*, vol. 6, pp. 118–120, Jan. 1994.

[32] B. E. A Saleh and M. C. Teich, *Fundamentals of Photonics*. New York: Wiley, 1991.

[33] S. Haykin and B. Van Veen, *Signals and Systems*. New York: Wiley, 1999.

[34] T. C. Cheston and J. Frank, "Phased array radar antennas," in *Radar Handbook*, M. Skolnik, Ed. New York: McGraw-Hill, 1990.

[35] A. K. Agrawal and E. L. Holzman, "Beamfromer architectures for active phased-array radar applications," *IEEE Trans. Antennas Propagat.*, vol. 47, pp. 432–442, Mar. 1999.

[36] R. J. Mailloux, "Array grating lobes due to periodic phase, amplitude, and time delay quantization," *IEEE Trans. Antennas Propagat.*, vol. AP-32, pp. 1364–1368, Dec. 1984.
[37] N. A. Riza, "Acousto-optic architecture for two-dimensional beam scanning in phased-array antennas," *Appl. Opt.*, vol. 31, no. 17, pp. 3278–3284, June 1992.

William D. Jemison (S'83–M'85–SM'96) received the B.S.E.E. degree from Lafayette College, Easton, PA, in 1985, the M.E.Sc. degree from Pennsylvania State University, University Park, in 1988, and the Ph.D. degree from Drexel University, Philadelphia, PA, in 1993.

In 1996, he joined the faculty of Lafayette College, where he teaches courses and laboratories in microwave systems, electromagnetics, electronics, analog and digital circuits, and control systems. Prior to 1996, he was a Senior Engineer and Project Manager at the Naval Air Warfare Center, Lockheed Martin Corporation, and Orbit/FR, where he worked in the field of microwave system design. He has authored or coauthored over 45 technical papers and coauthored one book chapter. He holds three U.S. patents. His current research interests are in the areas of microwave photonic systems, microwave circuits and antennas, and biological applications of microwaves and photonics.

Dr. Jemison is a member of Eta Kappa Nu.